HHS Public Access

Author manuscript

Part Part Syst Charact. Author manuscript; available in PMC 2020 August 27.

Published in final edited form as:

Part Part Syst Charact. 2019 August ; 36(8): . doi:10.1002/ppsc.201900171.

Copper Sulfide Nanodisks and Nanoprisms for Photoacoustic Ovarian Tumor Imaging

Junxin Wang[1], **Su-wen Hsu**[1], **Natalia Gonzalez-Pech**[2], **Anamik Jhunjhunwala**[3], **Fang Chen**[4], **Ali Hariri**[1], **Vicki Grassian**[1,2,4], **Andrea Tao**[1,2,4], **Jesse V. Jokerst**[1,4,5,*]

[1]Department of Nano Engineering, University of California San Diego, La Jolla, CA 92093, USA

[2]Department of Chemistry and Biochemistry, University of California San Diego, La Jolla, CA 92093, USA

[3]Department of Bioengineering, University of California San Diego, La Jolla, CA 92093, USA

[4]Material Science and Engineering Program, University of California San Diego, La Jolla, CA 92093, USA

[5]Department of Radiology, University of California San Diego, La Jolla, CA 92093, USA

Abstract

Transvaginal ultrasound is widely used for ovarian cancer screening but has a high false positive rate. Photoacoustic imaging provides additional optical contrast to supplement ultrasound and might be able to improve the accuracy of screening. Here, we report two copper sulfide (CuS) nanoparticles types (nanodisks and triangular nanoprisms) as the photoacoustic contrast agents for imaging ovarian cancer. Both CuS nanoprisms and nanodisks were ~6 nm thick and ~26 nm wide and were coated with poly(ethylene glycol) to make them colloidally stable in phosphate buffered saline (PBS) for at least 2 weeks. The CuS nanodisks and nanoprisms revealed strong localized surface plasmon resonances with peak maxima at 1145 nm and 1098 nm, respectively. Both nanoparticles types had strong and stable photoacoustic intensity with detection limits below 120 pM. The circular CuS nanodisk remained in the circulation of nude mice (n=4) and xenograft 2008 ovarian tumors (n=4) 17.9-fold and 1.8-fold more than the triangular nanoprisms, respectively. Finally, the photoacoustic intensity of the tumors from the mice (n=3) treated with CuS nanodisks

*Correspondence: jjokerst@ucsd.edu.

Conflicts of Interest

The authors declare no competing financial interest

Supporting Information

was 3.0-fold higher than the baseline. The tumors treated with nanodisks had a characteristic peak at 920 nm in the spectrum to potentially differentiate the tumor from adjacent tissues.

Graphical Abstract

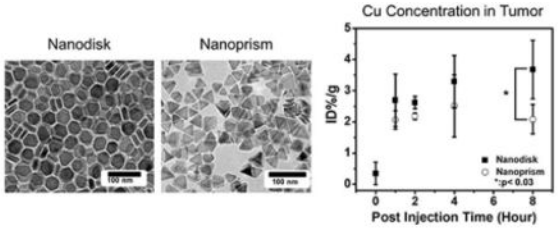

Copper sulfide nanodisks and nanoprisms are employed as photoacoustic contrast agents for ovarian tumor imaging. While these two nanoparticles have nearly identical length, thickness, and surface charge, nanodisks have 1.8-fold higher accumulation than nanoprisms in the xenograph human OV 2008 tumors. This difference indicates the importance of nanoparticle morphology for nanomedicine.

Keywords

Photoacoustic imaging; ovarian cancer; copper sulfide nanoparticles

1. Introduction

Photoacoustic imaging is an emerging modality for cancer diagnosis.[1] This ultrasound-based modality uses nanosecond laser pulses to generate thermal expansion leading to high frequency acoustic waves.[2] Photoacoustic imaging can increase the accuracy of ultrasound cancer imaging because it offers additional optical information/contrast. For example, hypoxic tumors have different photoacoustic spectra than normal tissues; thus, hemoglobin can be an endogenous photoacoustic contrast agent.[3]

Recent studies have demonstrated the potential of photoacoustic imaging to improve the accuracy of ovarian cancer screening in high risk populations.[4] Ovarian cancer has a poor prognosis with 60% of patients being diagnosed at late stages.[5] Transvaginal ultrasound imaging has been widely used for screening, but its positive-predictive value is only 5.3% suggesting false positives[6]. Thus, several groups have suggested that photoacoustic imaging could improve the value of imaging-based ovarian cancer screening. Zhu *et al.* have been developing photoacoustic imaging to improve the accuracy of ovarian cancer screening via classification algorithms that analyze the difference of photoacoustic spectra, envelopes, and images between benign and malignant ovarian tumors.[7] However, *in vivo* photoacoustic imaging studies in ovarian cancer are rare with a clinical sensitivity less than 90%.[7c, 8]

Nanoparticle-based photoacoustic contrast agents might further improve the sensitivity and specificity of screening by increasing the tumor signal. Examples include iron/silica/gold core−shell nanoparticles,[9] gold nanorods,[1e] and near-infrared dye-labeled magnetic iron

oxide nanoparticles.[10] In one example, mice received HER-2/neu targeted magnetic iron oxide nanoparticles had 5-fold higher photoacoustic intensity than mice without injection.[10]

More recently, copper sulfide nanoparticles, nanodisks[11] and nanoprisms[12] were shown to have tunable localized surface plasmon resonances (LSPRs) from 1000 to 1500 nm.[11–13] These wavelengths might facilitate deeper penetration depth (before water absorption increases) or could lead to multiplexed imaging of multiple data channels by expanding the range of usable wavelengths.[14] For example, CuS nanoparticles were imaged at 1064 nm in a rodent brain with intact skull as well as *in vitro* samples under 5 cm of chicken breast tissue.[15] In addition, the geometrics of these nanoparticles might also affect their extravasation in murine tumor models as described previously in comparisons between different nanoparticle shapes[16].

For these reasons, we evaluated CuS nanodisks and nanoprisms as photoacoustic contrast agents for ovarian cancer imaging. These materials have nearly identical dimensions, surface coatings, and surface charges with the exception of their different geometric shapes to test the shape effect of nanoparticle on the extravasation. We then used photoacoustic imaging and inductively coupled plasma mass spectrometry (ICP-MS) to study the photoacoustic properties and extravasation of CuS nanodisks and nanoprisms in xenograft ovarian tumor models. We characterized their photoacoustic intensities, limit of detection, signal stability, and accumulation efficiency in the mice bearing human OV2008 xenograft tumors. The data suggest that the CuS nanodisk are retained longer in the circulation with more accumulation in the tumors.

2. Results and Discussion

2.1 Synthesis and Characterization of CuS Nanodisks and Nanoprisms.

We used a solvent-based method to synthesize the CuS nanodisks and a seed/halide ion-mediated process for the synthesis of CuS nanoprisms (Fig. 1A).[12–13] The synthesis of CuS nanodisks employed Cu salt and S powder as reactants and oleylamine as a nanocrystal capping agent. The oleylamine activates the S powder precursor by forming oleylammonium hydrosulfide, which reacts with Cu^{2+} ions to precipitate CuS and form the disk-like CuS nanocrystals.[13] Nanoprism synthesis used CuS nanodisks as the seed, where added chloride ions promote the growth of facetted triangular nanoprisms.[12] The chloride ions cooperatively stabilize the low-index CuS surfaces and preferentially enhances the growth in and along a given crystallographic direction during synthesis. By carefully controlling the reaction time and temperature, we synthesized CuS nanodisks and nanoprisms with similar thicknesses and widths.

Figure 1B and 1C detail the morphology and size of the CuS nanoparticles. The average thickness of nanodisks and nanoprisms was 6.5 ± 0.7 nm and 6.3 ± 0.8 nm, respectively. TEM measurements indicated that the average diameter of the nanodisks was 25.6 ± 2.5 nm (PDI=0.256, measured by dynamic light scattering (DLS)), and the average edge length of the nanoprism was 26.8 ± 3.3 nm (PDI=0.247). These nanodisks and nanoprisms were

colloidally stable without aggregation in chloroform (nanodisk and nanoprism in Fig. 1D), but they precipitated in water because of the hydrophobic oleylamine coating (Fig. 1D inset).

We improved the hydrophilicity by substituting the surface coating with hydrophilic and biocompatible polyethylene glycol (PEG). We incubated the as-made CuS nanoparticles with PEG-thiol (Mw=5000) to form strong Cu-S bonds with the nanoparticles, which replaced the oleylamine. The hydrodynamic radius of the CuS nanodisks and nanoprisms in water increased from 85.3 to 125.4 nm and from 91.9 to 131.7 nm (Fig. 1D), respectively. The water-stable nanoparticles further confirmed the PEGylation on both CuS nanoparticles (Fig. 1D inset). Zeta potential measurements revealed the negative surface charge on these nanoparticles (−10.2 mV for the nanodisk and −10.5 mV for the nanoprism). A time-dependent, hydrodynamic radius measurement of the nanoparticles showed that both CuS nanodisk and nanoprism were stable for at least 2 weeks at room temperature (Supplementary Fig. S1).

We used TGA (Fig. S2) and absorbance data (Fig. S3) to estimate the number of particles per unit volume. Upon heating (> 400 °C), 0.172 μL CuS nanodisk colloidal solution resulted in 0.379 mg (bare CuS nanodisk). The molar concentration of the CuS nanodisks can be calculated as following: (1) one nanodisk volume with average diameter of 25.6 nm and thickness of 6.5 nm = $(25.6\ nm/2)^2 \times \pi \times (6.5\ nm)^2 = 3.34 \times 10^3\ nm^3$; (2) weight of one CuS nanodisk = $3.34 \times 10^3\ nm^3 \times 4.76\ g/cm$ (density of CuS) = 1.59×10^{-17} g; (3) number of CuS nanodisk in the test sample = 3.79×10^{-3} g/1.59×10^{-17} g= 2.38×10^{13}; (4) mole of CuS nanodisk in the test sample = $2.38 \times 10^{13} / 6.02 \times 10^{23}$ (Avogadro's number /mole) = 3.95×10^{-11} mole; (5) concentration of CuS nanodisk in the colloidal solution = 3.95×10^{-11} mole / 0.172×10^{-6} L= 2.30×10^{-7} M. Combined with Beer's law (extinction = molar extinction coefficient × path length × analyte concentration), the molar extinction coefficient can be calculated based on the extinction spectrum of the CuS nanodisk colloidal solution in Fig. S3 (diluted 200 times relative to the TGA sample). The molar extinction coefficient at 1145 nm = $0.4046 \times 200 / 2 \times 2.30 \times 10^{-7} = 3.52 \times 10^8\ M^{-1}cm^{-1}$, which is ~10 times lower than gold nanorod (2.5 to $5.5 \times 10^9\ M^{-1}cm^{-1}$)[17].

2.2 Photoacoustic Response of CuS Nanodisks and Nanoprisms

The PEGylated CuS nanodisks and nanoprisms had strong optical and photoacoustic absorption at near-infrared wavelengths. The maximum extinction intensity of the nanodisk and nanoprism occurred at 1145 and 1098 nm, respectively (Fig. 2A). The photoacoustic spectra of these two nanoparticles were slightly blue-shifted compared to their extinction spectra. Both types of CuS nanoparticles had maximum photoacoustic intensity at 945 nm, which is inconsistent with their absorption peaks. Indeed, the absorption and photoacoustic peaks should be identical because photoacoustic signal is based on absorption. The difference seen in Fig. 2A is because the laser on our photoacoustic scanner has a range of 680 to 970 nm; the laser power also decreases at more red-shifted wavelengths (Fig. S4). Nevertheless, both CuS nanodisks and nanoprisms had linear photoacoustic enhancement at 945 nm as a function of CuS concentration (R^2>0.97 for nanodisk and R^2>0.91 for nanoprism) (Fig. 2B). The detection limits (three standard deviations above background) of nanodisks and nanoprism were 29 pM and 116 pM, respectively (Fig. 2C). This is similar to

values reported previously for gold nanorods.[1e] The CuS nanodisks (RSD=0.84%) and nanoprisms (RSD=0.73%) also have stable signal and retain their structures under laser irradiation for 14 minutes—this is in sharp contrast to gold nanorods, which are known to deform at moderate laser fluence (Fig. S5).[18]

2.3 Nanoparticle Accumulation in Ovarian Tumor and the Photoacoustic Imaging

Using the similar physical properties of the two CuS nanoparticles, we next studied the shape effect of the CuS nanoparticles on their accumulation in ovarian tumors. We intravenously injected 200 μL 50 nM CuS nanoparticles (or 5.4 nM in the mouse body assuming the average blood volume of a mouse is 74 mL/kg[19]) in nude mice bearing OV2008 xenograft ovarian tumors. This was a safe dose because we found that the ovarian cancer cells had 95% viability after the incubation with 5 nM nanodisk for 24 hours (Fig. S6). Furthermore, this CuS nanoparticle concentration is 1425 times lower than the lethal dose of CuS nanoparticles (7.7 mM in the mouse body) reported by Feng *et al.*[20]. Other toxicity studies showed that a single dose below 4.2 mM of Cu[21] or 1.2 mM CuS nanoparticles[20] had minor toxicity in mice, even though Cu ions can be toxic at high concentration. This is because CuS nanoparticles have low solubility of free Cu.[21] The literatures suggest that CuS nanoparticles are relatively non-toxic. A detailed toxicity study of the CuS nanodisk and nanoprism was beyond the scope of this study. However, we used PEG-thiol to substitute for the oleylamine capping ligand similar to Guo *et al.* [(Ref. 21)], and this work suggested good biocompatibility.

The pharmacokinetic study used the Cu concentration in blood and tumor to evaluate tumor uptake and clearance. We first verified the Cu content in the nanodisks and nanoprisms on a per particle basis and found that the difference was 5.5%. The average Cu concentration in the blood from the mice (n=4) treated with nanodisks decreased from 42.5 to 18.6 ID%/g 8 hours after injection (Fig. 3A). The Cu concentration in the mice treated with nanoprisms decreased from 48.8 to 1.0 ID%/g (Fig. 3A). This indicated that the nanodisks had a longer circulation half-life than the nanoprisms.

The Cu concentration in the tumors treated with CuS nanodisks increased to 3.7 ID%/g 8-hour post-injection while the Cu concentration in the tumors treated with nanoprism initially increased to 2.5 ID%/g 4-hour post-injection and then decreased to 2.1 ID%/g 8-hour post-injection (Fig. 3B). The difference of Cu concentration in the tumors suggested that the circular CuS nanodisks had more retention in the 2008 ovarian tumors than the triangular CuS nanoprisms. The longer retention of the nanodisk in the ovarian tumors was likely a result of its long half-life (Fig. 3B). Other possible mechanisms include the strong adhesion of disk-like nanoparticles to the vascular wall and the geometry and size of the pore between the endothelial cells in the ovarian tumor.[16a-c] Although the underlying mechanism requires further investigation, this data provides insights in the selection of nanoparticles for ovarian tumor imaging and therapy.

The tumors from the mice treated with CuS nanodisk (n=3) exhibited a strong photoacoustic intensity with a characteristic photoacoustic spectral profile. The average photoacoustic intensity of the tumors 4 hours post-injection of CuS nanodisks was 3.0-fold ($p<0.01$, n=3) higher than the baseline (i.e. tumor without any treatment) (Fig. 3C). Furthermore, the

photoacoustic spectra of the tumors treated with CuS nanodisks had their maximum intensity at 920.0 ± 7.1 nm (Fig. 3D solid) with a spectral profile close to the nanodisk alone (Fig. 2A). In contrast, the baseline showed the maximum photoacoustic intensity at 713.3±2.4 nm (Fig. 3D dash), which was likely due to hemoglobin absorption.[22] The characteristic spectral peak at 920 nm could increase the contrast of the CuS nanoparticles in normal tissues by avoiding the interference of deoxygenated hemoglobin that has peak photoacoustic intensity at 750 nm.[23] The *in vivo* photoacoustic image in Supplementary Fig. S7 showed that the ultrasound signal can discriminate the tumor from adjacent tissues with the characteristic photoacoustic spectral information.

3. Conclusion

In summary, we report two CuS nanoparticle contrast agents, nanodisks and nanoprisms, for photoacoustic ovarian tumor imaging. Both CuS nanodisks and nanoprisms had sensitive photoacoustic signal at picomolar range, and the CuS nanodisks accumulate more in the human 2008 ovarian tumor models than the CuS nanoprisms. The photoacoustic image of the tumor treated with CuS nanodisks presented 3.0-fold higher intensity than the baseline and revealed a characteristic photoacoustic spectral peak at 920 nm.

4. Material and Methods:

4.1 Chemicals

Copper nitrate ($Cu(NO_3)_2 \cdot 2.5H_2O$) and chloroform were purchased from Fisher. Copper(II) chloride (97%), oleylamine (70%), 1-octadecene(90%), sulfur powder (99.99%), and copper ICP standard were purchased from Sigma-Aldrich. Ethanol (200 proof) was purchased form Goldshield Chemical. Poly(ethylene glycol) methyl ether thiol (PEG-thiol, Mw=5000) was purchased from Laysan Bio. Dulbecco's modified eagle medium (DMEM), fetal bovine serum, antibiotic-antimycotic (100X), and AlamarBlue® assay were purchased from Thermo Fisher Scientific. The internal standard for ICP was purchased from Inorganic Ventures. The nitric acid (70%) and hydrochloric acid (36.5–38%) was purchased from Fisher Scientific and J.T. Baker, respectively. Laboratory polyethylene tubing (OD: 1.27 mm, ID: 0.85 mm) was purchased from Harvard Apparatus, and 0.2 μm polyethersulfone syringe filters (Puradisc 25AS) were purchased from Whatman.

4.2 CuS nanodisks by solvent-based synthesis

The nanodisks were prepared as previously described[12–13] with minor adjustments. A 0.4 M copper nitrate solution was prepared by dissolving 0.0928 g copper nitrate (0.4 mmol) in 4 mL mixture solvent of oleylamine/1-octadecene (volume ratio of 1:3). Then, 0.0096 g (0.3 mmol) sulfur powder was added to the dark blue copper nitrate solution with stirring for 5 minutes. Next, the solution was placed in an oil bath at 180°C, and the solution color turned dark green/blue. The solution was cooled to room temperature to purify the nanodisks. Here, 4 mL ethanol was added to the as-made nanodisk solution, and the solution was centrifuged at 3000 rpm for 5 minutes to remove free oleylamine and 1-octadecene. The pellet was resuspended in chloroform and centrifuged at 7500 rpm for 7.5 minutes to remove any byproducts.

4.3 Shape focusing of triangular nanoprisms by seed-mediated growth

The seeds were prepared by adding 0.2 mmol copper (II) chloride and 0.3 mmol sulfur powder in a mixed solvent of 1 mL oleylamine and 3 mL 1-octadecene at 140 °C for 45 minutes. Next, 10% CuS seed solution (after purification to remove free oleylamine and byproducts) dispersed in 1-octadecene was added to the growth solution prepared by dissolving 0.05 mmol copper (II) chloride and 0.075 mmol sulfur powder in a mixed solvent (i.e. 0.25 mL oleylamine with 3.75 mL1-octadecene). The seed/growth mixed solution was placed in a 120°C oil bath for 75 minutes. After the bright-blue solution turned dark green-blue, the solution was cooled to room temperature. Then, 4 mL ethanol was added into the solution, and the solution was centrifuged at 3000 rpm for 5 minutes to remove the free oleylamine and 1-octadecene. The pellet was resuspended in chloroform and centrifuged at 7500 rpm for 7.5 minutes to remove any byproducts. These CuS nanoparticles were used as “new seeds”, and the synthesis process was repeated until the CuS nanocrystal grew to be the triangular nanoprism.

4.4 Surface modification of CuS nanodisks/nanoprisms

4 mL of oleylamine coated CuS nanodisks (or nanoprisms) in colloidal solution (in chloroform) was mixed with 1 mL 0.2 mM poly(ethylene glycol) methyl ether thiol (PEG-thiol, MW=5000) in a mixed solvent of chloroform/ethanol (volume ratio=1:1) and incubated at room temperature for 24 hours. The PEGylated nanodisks (or nanoprisms) were collected by centrifugation at 14,800 rpm for 45–60 minutes. The precipitation was resuspended in DI water and centrifuged at 14,800 rpm for 45–60 minutes to remove the free PEG-thiol twice; finally, the PEGylated nanodisks (or nanoprisms) were eventually dispersed in DI water or PBS solution.

4.5 Size measurement using transmission electron microscopy (TEM), atomic force microscopy (AFM), and dynamic light scattering (DLS)

The as-synthesized nanodisk and nanoprism were dispersed in chloroform and were incompatible with the carbon support film on commercial TEM grids. Therefore, we deposited the nanodisk or nanoprism solution onto air-water interface to evaporate the chloroform before transferring the nanoparticles to a TEM grid. The PEG-thiol coated nanodisks and nanoprisms dispersed in PBS solution were directly dripped onto the TEM grids. The TEM grids were kept in a vacutainer for at least 30 minutes to evaporate the water prior to TEM (JEOL 1200 EX II). The thickness of nanodisk was measured by TEM due to particle assemble by face-to-face interaction into larger nanostructure. The thickness of nanoprisms was measure by AFM.

The PEGylated nanodisks/nanoprisms were dissolved in deionized water for DLS (Malvern, Nano-ZS) measurements. Stability characterization used the same PEGylated nanodisks and nanoprisms and measured them every 2–3 days for 14 days.

4.6 CuS Thermogravimetric Analysis.

The molar extinction coefficient of the CuS nanocrystal in the CuS colloidal solution was calculated via the results from thermal gravimetric analysis (TGA, Perkin-Elmer TGA7) and the extinction spectrum of the CuS colloidal solution. 0.172 μL CuS nanodisk dispersed in

chloroform was heated to 400 °C under a nitrogen atmosphere resulting in bare CuS nanodisks. The concentration of the particle was calculated based on the resulted mass, density of CuS, size of the particles (i.e. width and thickness), and the absorbance of the sample at 1145 nm.

4.7 Absorbance and Photoacoustic Imaging Characterization

The absorbance spectra (700–1200 nm) of the nanodisks and nanoprisms dispersed in chloroform were collected with a PerkinElmer Lambda 1050 spectrophotometer.

The photoacoustic intensity and spectra of these samples were obtained via a Vevo LAZR imaging system (Visualsonics). The photoacoustic imaging system consists of a 21 MHz-centered transducer (bandwidth: 13–24 MHz) and a flashlamp pumped Q-switched Nd:YAG laser with an optical parametric oscillator and second harmonic generator. The system generates laser pulses (4–6 ns, 20Hz, 45±5 mJ, tunable wavelength 680–970 nm) and acquires acoustic waves induced by thermal expansion. The nanodisks/nanoprisms samples were injected in the polyethylene tubing fixed in a customized holder[24] and placed horizontally 10 mm under the transducer for maximized laser exposure. The photoacoustic images were acquired using the LZ250 transducer (21 MHz, bandwidth: 13–24 MHz) because it provided higher photoacoustic signal of the CuS nanoparticles than LZ201 (15 MHz, bandwidth: 9–18 MHz) and LZ550 (40 MHz, bandwidth: 32–55 MHz) (Supplementary Fig. S8). The full field-of-view of the photoacoustic images is 26 × 15 mm. The CuS nanodisk-treated ovarian tumors (4 hours post-injection) were imbedded in 1 wt.% agarose gel phantoms in a petri dish. The photoacoustic spectrum was normalized via dividing each intensity value by the maximum intensity value of the spectrum. For *in vivo* imaging confirmation, the mouse was imaged after the intravenous injection of 200 μL of 50 nM CuS nanodisk or PBS. The photoacoustic images were reconstructed using a maximum intensity projection, and the photoacoustic signal of the tumor volume was quantified using ImageJ [25].

4.8 Cell Culture and Cytotoxicity Studies

Human OV 2008 human ovarian cancer cells were acquired from ATCC and cultured in DMEM medium that contained 5% antibiotic-antimycotic and 10% fetal bovine serum. The cells were passaged 3 times prior to cytotoxicity test or tumor implantation. We seeded the cells in a 96 well plate at 10,000 cells per well and analyzed the wells in replicates (n=8). 100 μL nanodisk or nanoprism (5, 3, 2, 1, 0.5 nM) dissolved in cell culture medium, pure cell culture medium (0 nM), or 10% CTAB (dead cells, positive control) was incubated with the cells for 24 hours. After removing the medium and washing the cells with PBS for 3 times, the cells were treated with the alamarBlue® reagent (10% in cell culture medium) for 4 hours. The cell viability was determined by fluorescent measurement at 550 nm excitation and 580 nm emission.

4.9 Animal Studies

All animal work was conducted in accordance with the administrative panel of Animal Care Program of the University of California San Diego. The 6-week old female nude mice were randomly divided into 8 experimental groups. To implant the tumors in the mice, 5–10

million human 2008 ovarian cells mixed with 100 μL growth factor reduced Matrigel were subcutaneously injected into the hind limb of a mouse. When the tumor grew to ~1.0 cm long, 200 μL of 20 nM CuS nanodisk or nanoprism prepared in PBS was injected into the tail vein of a mouse. The groups were studied at 1, 2, 4, or 8 hours (n = 4 mice per group). The total number of mice for the CuS nanodisk and nanoprism treatment groups was 32 (4 groups × 4 animals/group × 2 nanoparticle types). After incubation for 1, 2, 4, or 8 hours, 0.5–1 mL blood was collected via cardiac puncture, and the tumor was excised for ICP-MS analysis and photoacoustic imaging. Three sets of blood and tumor samples from mice without any treatment were used as the negative control to determine baseline concentrations.

4.10 Measurement of Copper Concentration in Blood and Tumor

The copper concentrations in blood and tumors were measured by ICP-MS (iCAP RQ ICP-MS, Thermo Fisher Scientific, Waltham, MA, USA). All samples were weighed and added to Teflon vessels. The samples were spiked with the internal standard solution and then digested in 10 mL of *aqua regia* using a MARS 6 microwave digestion system (CEM Corporation, Matthews, NC). The program used included the following: (1) 45-minute ramp to 150 °C, (2) 45-minute hold, (3) 30-minute cooling ramp to 50 °C, (4) 45-minute ramp to 195 °C, (5) 45 minutes of hold, and (6) a 25-minute cooling ramp to 30 °C. After the digestion was complete, all the samples were transferred into volumetric flask (25 mL) and allowed to degas under the fume hood for 30 minutes and then diluted to 25 mL using milliQ water. The digested samples were filtered with 0.2 μm polyethersulfone syringe filters. A final 1:10 dilution was carried out with 2% nitric acid. ICP-MS analysis was carried out for Cu using copper standard solutions (0, 1, 2, 5, 10, 20, 50, 100 ppb). All samples were analyzed in triplicate.

4.11 Data Analysis and Statistical Treatment.

The average and standard deviation of the integrated density were calculated using Microsoft excel functions “AVERAGE” and “STDEV”. The p-value was calculated via the two-tailed test using the Microsoft excel function, “TTEST”.

Supplementary Material

Refer to Web version on PubMed Central for supplementary material.

Acknowledgement

We acknowledge funding from NIH HL117048, HL137187, and infrastructure from S10 OD021821. The electron micrographs were taken in the Cellular and Molecular Medicine Electron microscopy core facility which is supported in part by NIH award S10 OD023527. The ICP-MS analysis was done in the Environmental Complex Analysis Laboratory on the UC San Diego campus.

Reference

[1]. a) Oraevsky A, Biomedical Photonics Handbook 2014, 715;b) Lyu Y, Zeng J, Jiang Y, Zhen X, Wang T, Qiu S, Lou X, Gao M, Pu K, ACS nano 2018, 12, 1801; [PubMed: 29385336] c) Wong TT, Zhang R, Hai P, Zhang C, Pleitez MA, Aft RL, Novack DV, Wang LV, Science Advances 2017, 3, e1602168; [PubMed: 28560329] d) Bohndiek SE, Sasportas LS, Machtaler S, Jokerst JV,

Hori S, Gambhir SS, Journal of Nuclear Medicine 2015, 56, 1942; [PubMed: 26315834] e) Jokerst JV, Cole AJ, Sompel D. Van de, Gambhir SS, ACS nano 2012, 6, 10366; [PubMed: 23101432] f) Mallidi S, Luke GP, Emelianov S, Trends in biotechnology 2011, 29, 213; [PubMed: 21324541] g) Heijblom M, Piras D, Engh F. M. van den, Schaaf M. van der, Klaase JM, Steenbergen W, Manohar S, European Radiology 2016, 26, 3874; [PubMed: 26945762] h) Valluru KS, Willmann JK, Ultrasonography 2016, 35, 267; [PubMed: 27669961] i) Muhanna N, Jin CS, Huynh E, Chan H, Qiu Y, Jiang W, Cui L, Burgess L, Akens MK, Chen J, Irish JC, Zheng G, Theranostics 2015, 5, 1428; [PubMed: 26681987] j) Wilson KE, Bachawal SV, Abou-Elkacem L, Jensen K, Machtaler S, Tian L, Willmann JK, Theranostics 2017, 7, 1463; [PubMed: 28529630] k) Chitgupi U, Lovell JF, Biomedical Engineering Letters 2018, 1; [PubMed: 30603186] l) Xu C, Chen F, Valdovinos HF, Jiang D, Goel S, Yu B, Sun H, Barnhart TE, Moon JJ, Cai W, Biomaterials 2018, 165, 56. [PubMed: 29501970]

[2]. a) Tomaszewski MR, Gonzalez IQ, O'Connor JP, Abeyakoon O, Parker GJ, Williams KJ, Gilbert FJ, Bohndiek SE, Theranostics 2017, 7, 2900; [PubMed: 28824724] b) Bayer CL, Wlodarczyk BJ, Finnell RH, Emelianov SY, Biomed. Opt. Express 2017, 8, 757; [PubMed: 28270982] c) Hariri A, Wang J, Kim Y, Jhunjhunwala A, Chao DL, Jokerst JV, 2018;d) Jiang Y, Pu K, Accounts of chemical research 2018, 51, 1840; [PubMed: 30074381] e) Li J, Pu K, Chemical Society reviews 2019, 48, 38. [PubMed: 30387803]

[3]. a) Mehrmohammadi M, Joon Yoon S, Yeager D, Emelianov SY, Current Molecular Imaging 2013, 2, 89; [PubMed: 24032095] b) Anderson PG, Kainerstorfer JM, Sassaroli A, Krishnamurthy N, Homer MJ, Graham RA, Fantini S, PloS one 2015, 10, e0117322. [PubMed: 25781469]

[4]. Jacobs IJ, Menon U, Ryan A, Gentry-Maharaj A, Burnell M, Kalsi JK, Amso NN, Apostolidou S, Benjamin E, Cruickshank D, The Lancet 2016, 387, 945.

[5]. Howlader N NA, Krapcho M, Miller D, Bishop K, Kosary CL, Yu M, Ruhl J, Tatalovich Z, Mariotto A, Lewis DR, Chen HS, Feuer EJ, Cronin KA (eds), National Cancer Institute, Bethesda, MD based on November 2016 SEER data submission, posted to the SEER web site.

[6]. Menon U, Gentry-Maharaj A, Hallett R, Ryan A, Burnell M, Sharma A, Lewis S, Davies S, Philpott S, Lopes A, Godfrey K, Oram D, Herod J, Williamson K, Seif MW, Scott I, Mould T, Woolas R, Murdoch J, Dobbs S, Amso NN, Leeson S, Cruickshank D, McGuire A, Campbell S, Fallowfield L, Singh N, Dawnay A, Skates SJ, Parmar M, Jacobs I, The Lancet Oncology 2009, 10, 327. [PubMed: 19282241]

[7]. a) Salehi HS, Kumavor PD, Li H, Alqasemi U, Wang T, Xu C, Zhu Q, Photoacoustics 2015, 3, 114; [PubMed: 26640774] b) Li H, Kumavor P, Alqasemi US, Zhu Q, 2015;c) Salehi HS, Li H, Merkulov A, Kumavor PD, Vavadi H, Sanders M, Kueck A, Brewer MA, Zhu Q, 2016;d) Aguirre A, Ardeshirpour Y, Sanders MM, Brewer M, Zhu Q, Translational Oncology 2011, 4, 29; [PubMed: 21286375] e) Salehi HS, Wang T, Kumavor PD, Li H, Zhu Q, Biomed. Opt. Express 2014, 5, 3074. [PubMed: 25401021]

[8]. Nandy S, Mostafa A, Hagemann IS, Powell MA, Amidi E, Robinson K, Mutch DG, Siegel C, Zhu Q, Radiology 0, 180666.

[9]. Monaco I, Arena F, Biffi S, Locatelli E, Bortot B, La Cava F, Marini GM, Severini GM, Terreno E, Comes Franchini M, Bioconjugate chemistry 2017, 28, 1382. [PubMed: 28453929]

[10]. Xi L, Satpathy M, Zhao Q, Qian W, Yang L, Jiang H, Nanomedicine: Nanotechnology, Biology and Medicine 2014, 10, 669.

[11]. Hsu S-W, On K, Tao AR, Journal of the American Chemical Society 2011, 133, 19072. [PubMed: 22044349]

[12]. Hsu S-W, Ngo C, Bryks W, Tao AR, Chemistry of Materials 2015, 27, 4957.

[13]. Hsu S-W, Ngo C, Tao AR, Nano Letters 2014, 14, 2372. [PubMed: 24738726]

[14]. Kobat D, Durst ME, Nishimura N, Wong AW, Schaffer CB, Xu C, Opt. Express 2009, 17, 13354. [PubMed: 19654740]

[15]. Ku G, Zhou M, Song S, Huang Q, Hazle J, Li C, ACS nano 2012, 6, 7489. [PubMed: 22812694]

[16]. a) Smith BR, Kempen P, Bouley D, Xu A, Liu Z, Melosh N, Dai H, Sinclair R, Gambhir SS, Nano letters 2012, 12, 3369; [PubMed: 22650417] b) Chauhan VP, Popović Z, Chen O, Cui J, Fukumura D, Bawendi MG, Jain RK, Angewandte Chemie International Edition 2011, 50, 11417; [PubMed: 22113800] c) Adriani G, de Tullio MD, Ferrari M, Hussain F, Pascazio G, Liu

X, Decuzzi P, Biomaterials 2012, 33, 5504; [PubMed: 22579236] d) Toy R, Peiris PM, Ghaghada KB, Karathanasis E, Nanomedicine 2014, 9, 121. [PubMed: 24354814]

[17]. Orendorff CJ, Murphy CJ, The Journal of Physical Chemistry B 2006, 110, 3990. [PubMed: 16509687]

[18]. Link S, Burda C, Nikoobakht B, El-Sayed MA, The Journal of Physical Chemistry B 2000, 104, 6152.

[19]. Rahavendran SV, Vekich S, Skor H, Batugo M, Nguyen L, Shetty B, Shen Z, Bioanalysis 2012, 4, 1077. [PubMed: 22612688]

[20]. Feng W, Nie W, Cheng Y, Zhou X, Chen L, Qiu K, Chen Z, Zhu M, He C, Nanomedicine: Nanotechnology, Biology and Medicine 2015, 11, 901.

[21]. Guo L, Panderi I, Yan DD, Szulak K, Li Y, Chen Y-T, Ma H, Niesen DB, Seeram N, Ahmed A, Yan B, Pantazatos D, Lu W, ACS nano 2013, 7, 8780. [PubMed: 24053214]

[22]. Wilson RH, Nadeau KP, Jaworski FB, Tromberg BJ, Durkin AJ, 2015.

[23]. Rajian JR, Carson PL, Wang X, Opt. Express 2009, 17, 4879. [PubMed: 19293919]

[24]. Arconada-Alvarez SJ, Lemaster JE, Wang J, Jokerst JV, Photoacoustics 2017, 5, 17. [PubMed: 28239554]

[25]. Abràmoff MD, Magalhães PJ, Ram SJ, Biophotonics international 2004, 11, 36.

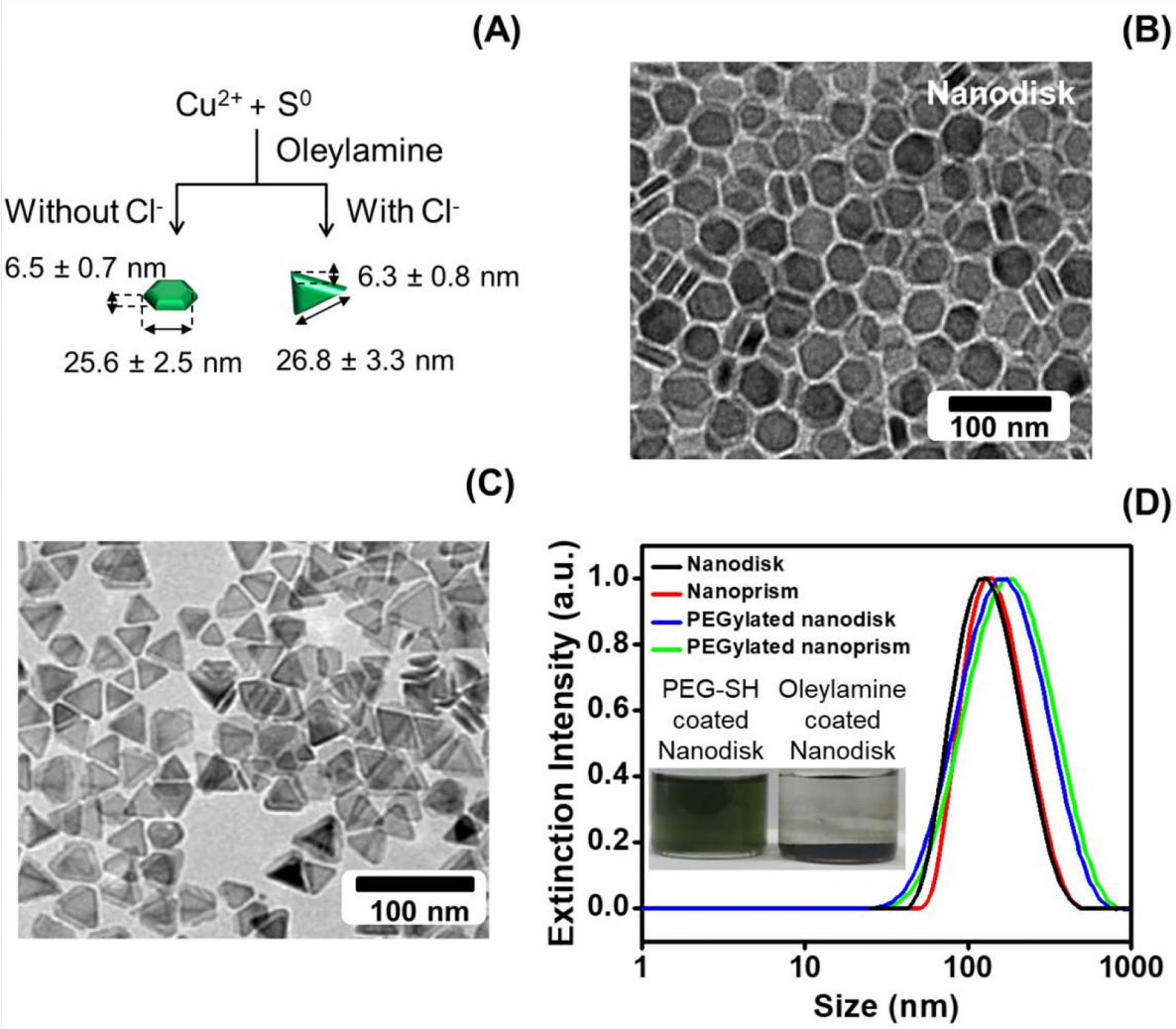

Figure 1: Physical and chemical characterization of CuS nanodisks and nanoprism.

Panel A depicts the synthesis of CuS nanodisks and nanoprisms via a solvent-based and seed/halide ion-mediated process. Panels B and C are the TEM images of the CuS nanodisks and nanoprisms, respectively. The average diameter and thickness of CuS nanodisk was 25.6 nm and 6.5 nm. The nanoprism was 26.8 wide and 6.3 nm thick. Panel D shows the hydrodynamic radius of the oleyamine-coated nanodisks (85.3 nm) and nanoprisms (91.9 nm) in chloroform. The hydrodynamic radius of the PEGylated nanodisks and nanoprism dissolved in water increased to 125.4 and 131.7 nm, respectively. While the oleynamine-coated CuS nanodisks precipitate in water, PEGylation stabilizes the nanodisk in water (inset). The size difference between TEM and DLS is caused by the DLS algorithm that is optimized for spherical particles and is a potential error source.

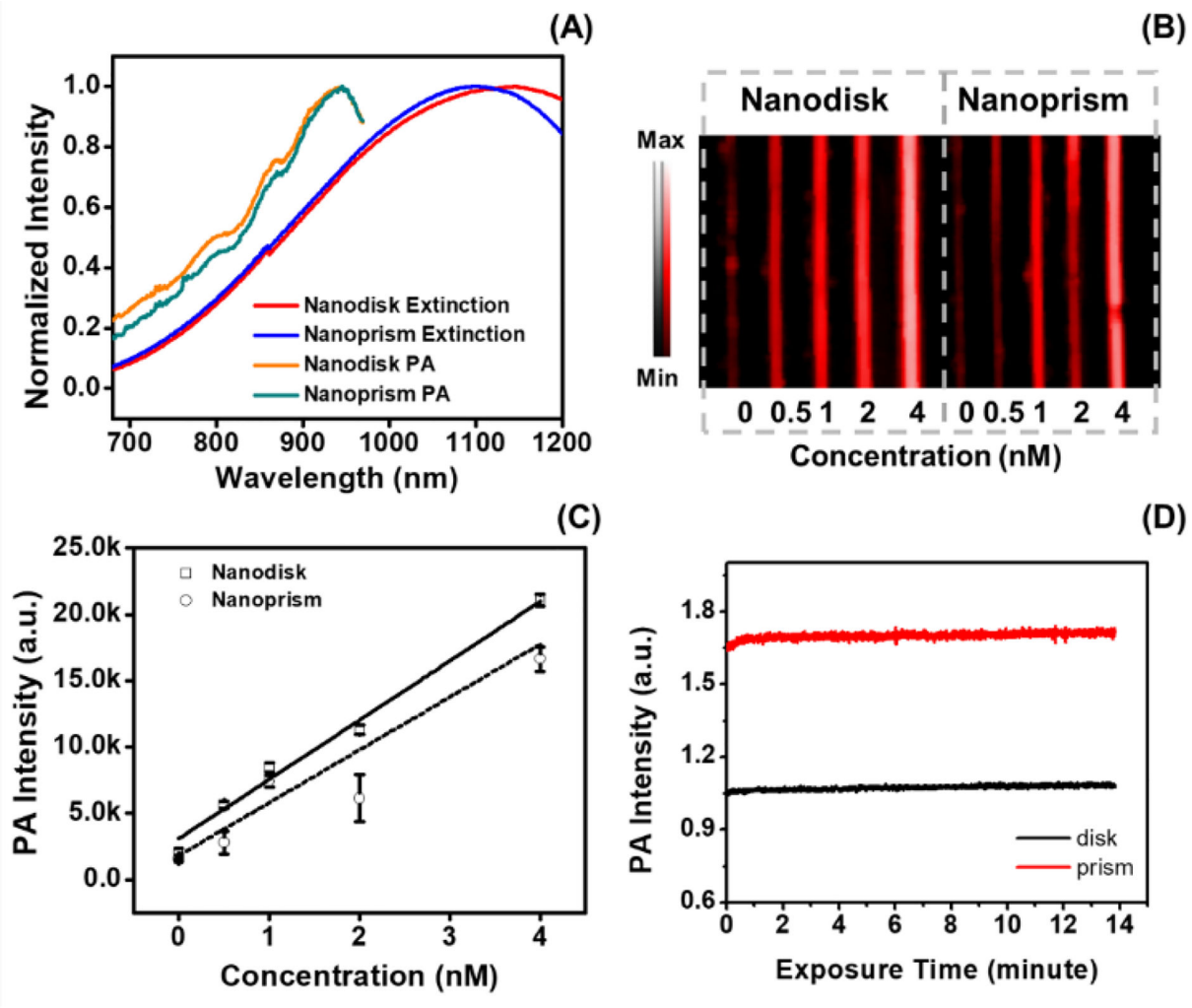

Figure 2: Photoacoustic signal capabilities of CuS nanodisks and nanoprisms.

Panel A compares the extinction spectra with the photoacoustic spectra of CuS nanodisks and nanoprisms. The extinction peak of nanodisks and nanoprisms was 1145 and 1098 nm, respectively, and both CuS nanoparticles had maximum photoacoustic output at 945 nm. The derivation of peak intensity between photoacoustic and extinction spectrum is due to the limited range of our laser (680 to 970 nm) and the lower laser energy at further infrared wavelengths (Fig. S4). The photoacoustic intensity measured at 945 nm of the two CuS nanoparticles is shown in B. The corresponding intensity analysis shown in C revealed the linear correlation between the photoacoustic intensity and the concentration of the nanodisks (solid line, R^2>0.97) and nanoprism (dashed line, R^2>0.91). Panel D highlights the stability of CuS nanodisk (RSD=0.84%) and nanoprism (RSD=0.73%) over a 14-minute laser irradiation at 940 nm. Error bars in panel C and D represents standard deviation of 8 regions of interest.

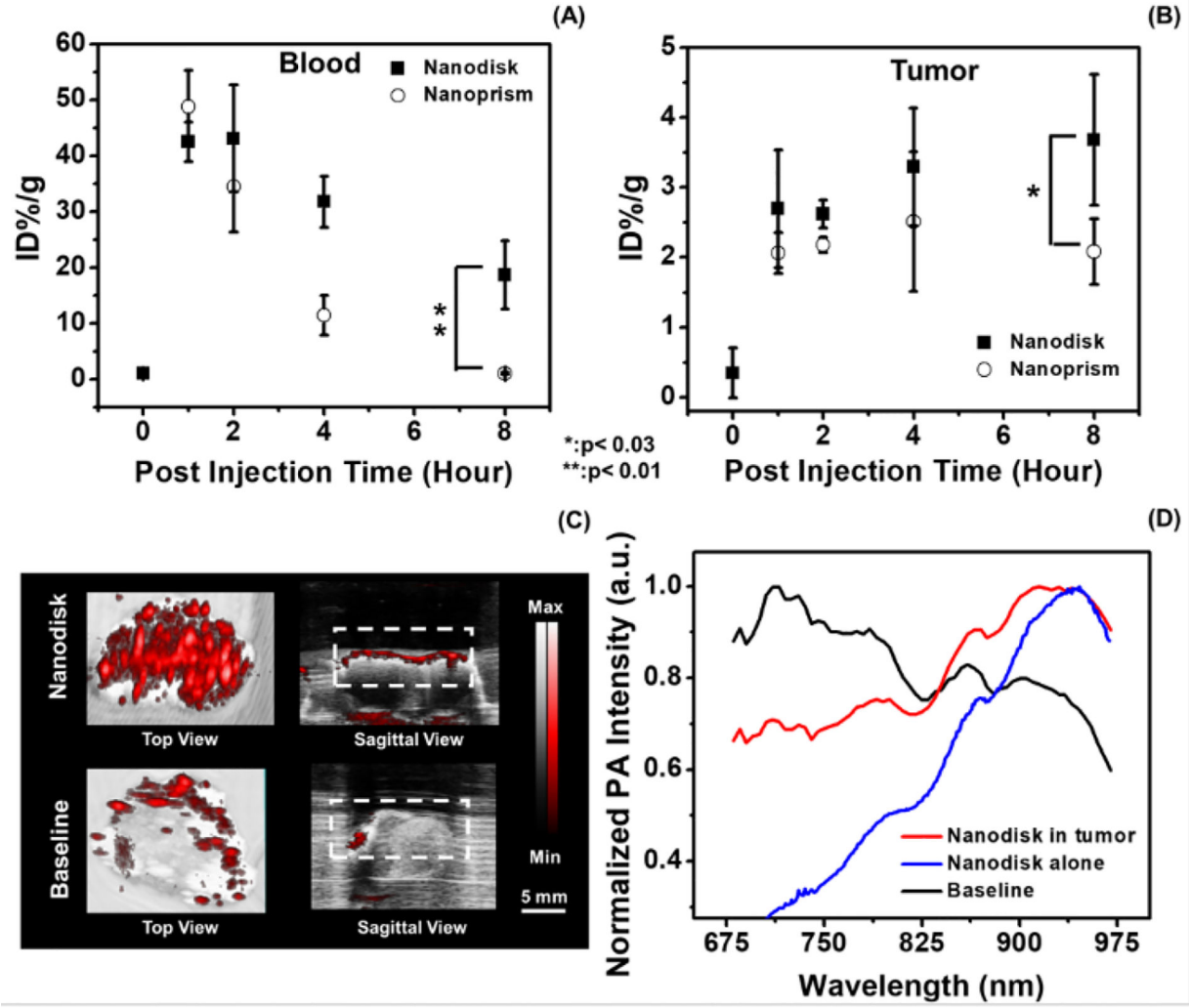

Figure 3: Shape-dependent accumulation of nanoparticles in tumor and photoacoustic ovarian tumor imaging.

Panel A and B shows the Cu ion concentration of the blood and tumor samples collected from mice treated with CuS nanodisks and nanoprisms, respectively. Eight hours after the treatment, the mice treated with nanodisk had 17.9-fold and 1.8-fold higher Cu concentration in the blood and tumor than the mice treated with nanoprisms. Here the data points at baseline represent the tumor without any nanoparticle treatment. The error bars in panel A and B denote the standard deviation from 4 mice. Panel C showed the photoacoustic images at 920 nm excitation of the tumor samples from the mice treated with CuS nanodisk (Nanodisk) and the mice without treatment (Baseline). The white dash line labels the regions of interest for the photoacoustic spectral analysis (D). The photoacoustic spectral profile of the tumor treated with the nanodisk agrees well with the nanodisk particles alone. The animals treated with CuS nanodisks revealed a maximum photoacoustic signal at 920 nm while the untreated tumors showed a maximum intensity at 713 nm.